iScience

CellPress
OPEN ACCESS

Article

Research on radiation field and driving based on super-low frequency mechanical antenna array

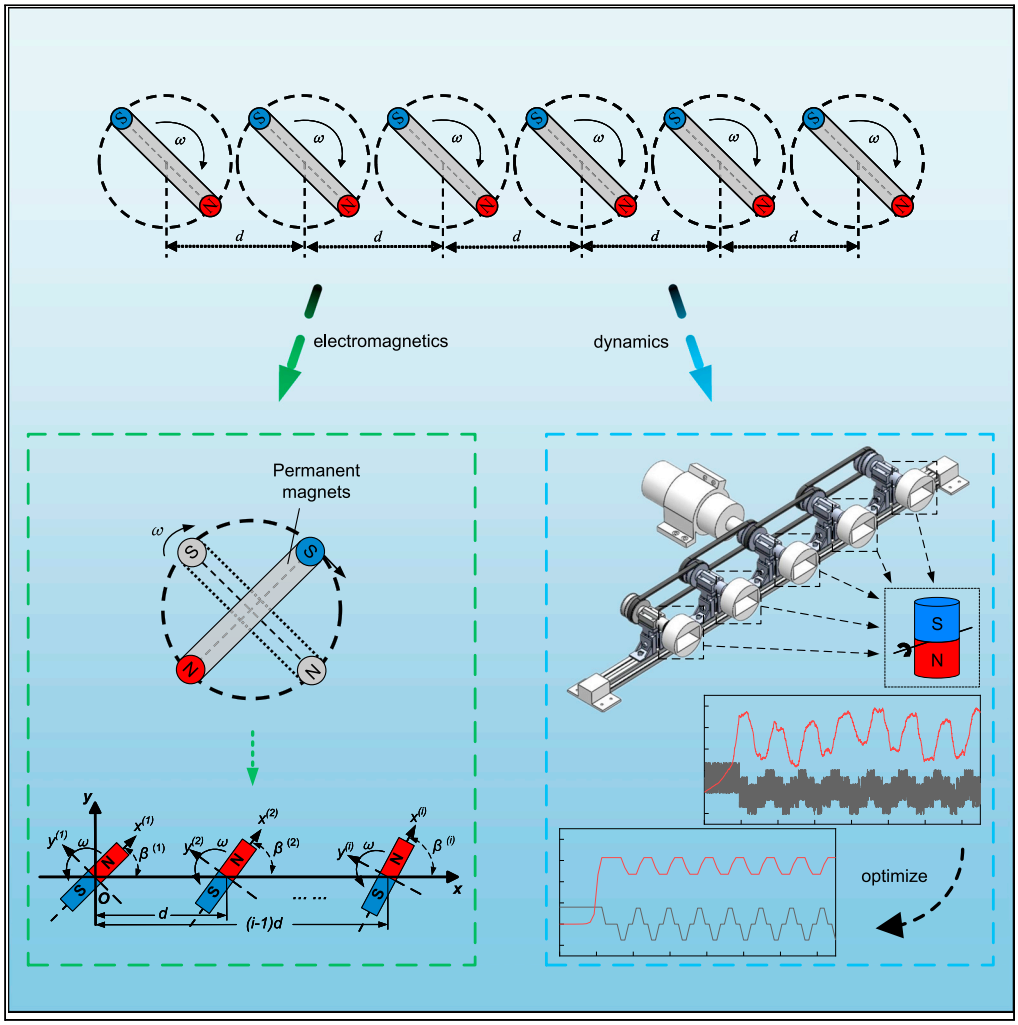

Xiaoyu Wang, Xijie Yang, Ziyi Li, Boyan Zhang, Zhenxin Cao

xiaoyuw@djtu.edu.cn

Highlights

Extending low frequency communication range using antenna arrays

Modeling the magnetics and mechanics of the antenna array

Establishing a more accurate 2FSK-based drive model to improve signal quality

Establishing the relationship between the array parameters and the radiation field

Wang et al., iScience 26, 106741
May 19, 2023
https://doi.org/10.1016/j.isci.2023.106741

iScience

CellPress
OPEN ACCESS

Article

Research on radiation field and driving based on super-low frequency mechanical antenna array

Xiaoyu Wang,[1,3,4,*] Xijie Yang,[1,3] Ziyi Li,[1] Boyan Zhang,[1] and Zhenxin Cao[2]

SUMMARY

Mechanical antennas (MAs) directly use the mechanical motion of electric or magnetic charges to excite electromagnetic waves. The radiation distance of rotating magnetic dipole type mechanical antennas is related to the volume of the radiation source, so the volume of the radiation source is too large for long-distance communication. To solve the above problem, we first establish the magnetic field model and differential equations of motion of the antenna array. Then, we design the prototype of antenna array with operating frequency of 75–125Hz. Finally, we experimentally established the radiation intensity relationship between a single permanent magnet and an array of permanent magnets. The results indicate that our driving model reduces the tolerance of the signal by 47%. Through 2FSK communication experiments, this article verifies the feasibility of extending the communication distance in the form of an array, which provides an important reference for long-distance low-frequency communication.

INTRODUCTION

Owing to their low attenuation in lossy media, superlow frequency (SLF) band electromagnetic waves have great application potential in ultra-long distance communication, air-water cross-domain communication, navigation, positioning, and other fields.[1–4] The traditional electrically small antenna (ESA) relies on the oscillating current in the conductor to excite electromagnetic waves. Its physical size is proportional to the wavelength, which makes the ESA low-frequency electromagnetic transmission system have problems such as large antenna size, complex equipment, low radiation efficiency, and large energy consumption.[5]

A rotating permanent magnet mechanical antenna does not need an impedance matching network and is not limited by the theoretical limit of ESA. It directly converts mechanical energy into electromagnetic energy through the mechanical drive structure. Also, the mechanical antenna uses permanent magnetic material as the radiation source, which can store constant electromagnetic energy,[6] further reducing the power demand of the input system.

Scholars from both home and abroad have conducted preliminary research and developed primary verification prototypes to evaluate the radiation ability of the super low frequency mechanical antenna. Gong et al. of Xidian University studied the radiation field and propagation coefficient of the antenna and the propagation law in different media.[7] Shi Wei et al. of the 63rd Research Institute of the National University of Defense Technology deduced the analytical formula of electromagnetic radiation from rotating permanent magnets[8,9] and verified through experiments that the magnetic field strength can be increased by 3 dB after two permanent magnet arrays. Hunter C. Burch et al. of the University of Florida demonstrated that mechanical antennas could generate time-varying magnetic fields by creating a prototype and conducting experiments,[10] as well as examining the relationship between magnetic field attenuation and communication distance. Selvin et al. of UCLA studied the electromagnetic radiation mechanism of permanent magnet rotation and the constraint relationship between the mechanical energy and magnetic energy of the antenna[11,12] and gave the corresponding limit formula of Q value. James A. Bickford et al. of Tufts University analyzed the field distribution of several mechanical antennas[13] and compared the performances of mechanical antennas, traditional ESAs, and coil transmitters through simulation, finding that the former's performance is more than 8 orders of magnitude higher. Matthew J. Brandsema et al. of the ARL have derived an accurate field mathematical model of a rotating oscillating charged thin spherical shell radiating low-frequency electromagnetic waves, which can be used to analyze radiation patterns, radiation efficiency, and spectral output.[14]

[1]School of Mechanical Engineering, Dalian Jiaotong University, Dalian, Liaoning 116028, China

[2]School of Information Science and Engineering, Southeast University, Nanjing, Jiangsu 210096, China

[3]These authors contributed equally

[4]Lead contact

*Correspondence: xiaoyuw@djtu.edu.cn

https://doi.org/10.1016/j.isci.2023.106741

For the scheme of designing low frequency mechanical antenna using new piezoelectric and magnetostrictive materials, domestic and foreign scholars have also conducted related research. A team from Beijing University of Posts and Telecommunications has studied piezoelectric mechanical antennas, and they designed mechanical antennas using piezoelectric ceramic rings[15] and relaxed ferroelectric ceramics (PMN-PT),[16] respectively, and verified the performance of the antennas through experiments. The team from Northeastern University studied the magnetoelectric mechanical antenna. They investigated the antenna with three-layer stacked structure[17] and suspended ferromagnetic/piezoelectric thin-film heterostructure,[18] established the analytical model of radiation field versus distance, and demonstrated experimentally that their antenna can improve the antenna gain by 50 dB. Compared with the rotating permanent magnet type mechanical antenna, the driving source of magneto-mechanical-electric coupled mechanical antenna is piezoelectric or magnetoelectric material, the main research focus is on the heterogeneous structure of multiple materials, and the requirements for new materials are higher.

In general, the mechanical antenna is still in the laboratory research stage. Through the use of a small volume permanent magnet, each team preliminary validated the feasibility of using mechanical antennas for super-low-frequency communication.[19] The radiation distance of a rotating permanent magnet mechanical antenna is limited by the performance parameters and volume of permanent magnet materials. At present, the performance of NdFeB and other third-generation rare-earth permanent magnetic materials has approached its theoretical limit.[20,21] However, increasing the permanent magnet volume will bring great challenges to the permanent magnet technology and antenna drive system. Therefore, this article proposes to decompose a single large-volume permanent magnet into multiple small-volume components to form an antenna array for ultra-long-distance low-frequency communication.

In the first section of this article, the radiation field model of the antenna array is derived, and the influence of key array parameters on the near-field radiation efficiency of the antenna is analyzed. In the second section, the kinematic differential equation of the system is established, the torque model of the electromechanical drive system of the antenna is optimized, and the frequency tolerance of the communication signal is reduced. In the third section, the experimental prototype of an antenna array is developed. The influence of array parameters is explored through experiments, and the electromechanical performance of the system's stable driving model and 2FSK modulation communication are verified.

Array radiation field model

Based on the radiation theory of permanent magnet mechanical antenna unit, when the receiving sensitivity is 100 *fT*@75Hz and 5 km distance communication is realized in the air domain, a permanent magnet with a volume of 200 dm^3 and a remanence of 1.5T is required.[22] This brings great challenges to the processing technology of permanent magnets and electromechanical drive systems.[23] To solve the above problems, this article proposes a method of using multiple small permanent magnets to form an antenna array to achieve remote communication.

The main form of antenna array is a plane array. As shown in Figure 1, the separable rectangular grid rectangular boundary plane array can be seen as some linear arrays arranged in rows or columns. Linear array analysis is the basis of planar array analysis. It includes two basic linear arrays: the array whose rotation planes are parallel to each other is called parallel linear array and the array whose rotation planes are coplanar is called coaxial linear array. The magnetic field coupling of each element of the latter is more complex, so the next step will focus on this array form.

In this chapter, the radiation field model of permanent magnet array is derived by using the inverse solution of position and attitude in space and the vector superposition theory. Based on this model, the influence of the antenna element spacing and the number of elements on the total radiation field intensity is analyzed, and the spatial propagation directivity of the radiation field of the antenna array is explored.

Analytical model of radiation field of coaxial linear array

According to the basic theorem of electromagnetic field and the perturbation theory of static magnetic field, the magnetic induction intensity expression of the radiation field of the rotating magnetic dipole in space can be obtained as:[24]

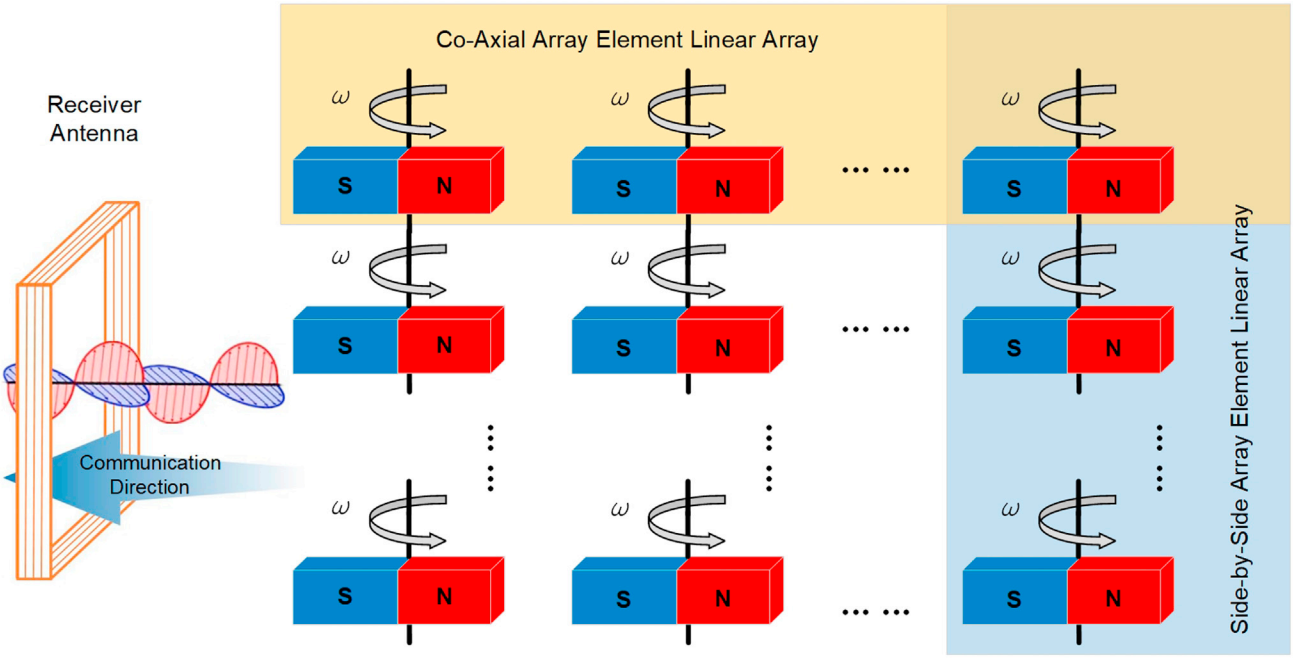

Figure 1. The basic morphological decomposition of a planar array of separable rectangular grids with rectangular boundaries

$$\overrightarrow{B_{mrot}(t)} = \frac{B_0 V}{4\pi R^3}\left[2\sin\theta\cos(\varphi+\omega t)\overrightarrow{a_R} - \cos\theta\cos(\varphi+\omega t)\overrightarrow{a_\theta} - \sin(\varphi+\omega t)\overrightarrow{a_\varphi}\right] \quad \text{(Equation 1)}$$

Where: B_0 is the remanence of the permanent magnet material; V is the volume of the permanent magnet array; R is the distance between the observation point and the rotation center of the permanent magnet; θ is the polar angle, which is the included angle between the measuring point and the positive direction of the z axis after connecting it with the origin; φ is the azimuth angle, which is the included angle between the projection on the xy plane and the positive direction of the x axis after the line between the observation point and the rotation center of the permanent magnet; $\overrightarrow{a_R}$, $\overrightarrow{a_\theta}$, and $\overrightarrow{a_\varphi}$ are the unit vectors corresponding to the lower corner parameters in the spherical coordinate system, respectively.

The analytical model of coaxial array is shown in Figure 2, with the element spacing d and the number of elements n. Establish the global coordinate system O-xyz, and the local coordinate system $O^{(i)}$-$x^{(i)}y^{(i)}z^{(i)}$ (i = 1,2, $\cdots$,n) rotating with each magnet array. Both the z axis of the global and local coordinate systems is vertically facing outward, and the origin of the local coordinate system is the geometric center of the magnet. The center of rotation of each element is in the positive x *axis* direction of the global coordinate system, and the first element is at the origin of the global coordinate system. The angle between the permanent magnet array element at the initial position and the positive x axis direction of the global coordinate system is $\beta^{(i)}$ (that is, the initial phase angle). Therefore, when the elements rotate around their respective axes of rotation $z^{(i)}$ at angular velocity ω to the t moment, the positive angle with respect to the x axis of the global coordinate system is:

$$\gamma(t)^{(i)} = \omega t + \beta^{(i)} \quad \text{(Equation 2)}$$

This gives the time-varying magnetic field generated by any array element i in its local coordinate system as:

$$\overrightarrow{B_{rot}(t)^{(i)}} = \frac{B_0 V}{4\pi R^3}\left[2\sin\theta\cos\left(\varphi^{(i)}+\gamma(t)^{(i)}\right)\overrightarrow{a_R} - \cos\theta\cos\left(\varphi^{(i)}+\gamma(t)^{(i)}\right)\overrightarrow{a_\theta} - \sin\left(\varphi^{(i)}+\gamma(t)^{(i)}\right)\overrightarrow{a_\varphi}\right] \quad \text{(Equation 3)}$$

To analyze the regulation effect of element spacing and number of elements on the radiation field intensity, it is necessary to establish a superimposed radiation field model of the coaxial array linear array based on the radiation model of the single rotating element mentioned above.

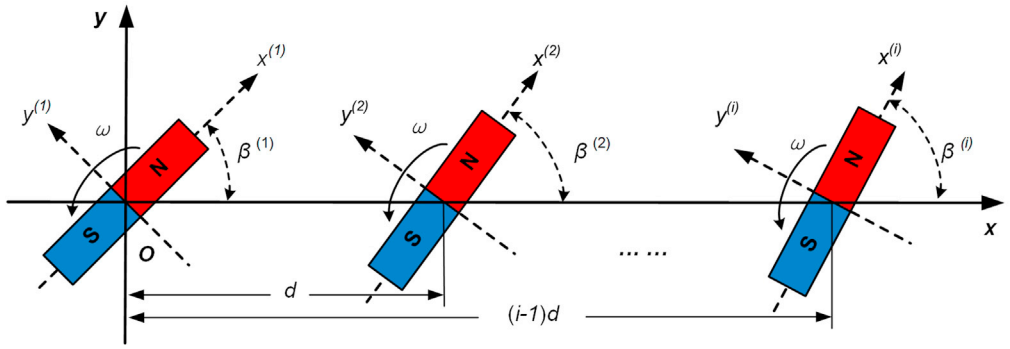

Figure 2. Analytical model of coaxial linear array

The static magnetic field strength of a permanent magnet in any position in free space can be equivalent to decompose into a horizontal magnetic field strength and a vertical magnetic field strength.[25] A stationary permanent magnet whose magnetic induction intensity B is line integral along any closed path is equal to the algebraic sum of the individual currents enclosed by this closed path multiplied by the permeability. From this, it can be deduced that the vertex is located at the origin of the coordinates of a stationary permanent magnet, and the expression of the magnetic induction intensity of $P(x,y,z)$ at any point in space is:

$$\vec{B} = B_x \vec{i} + B_y \vec{j} + B_z \vec{k} \quad \text{(Equation 4)}$$

Where the magnetic induction intensity in the three orthogonal directions of point P is:[26]

$$\begin{cases} B_x = -\dfrac{J_0}{4\pi}\sum_{i=1}^{2}\sum_{j=1}^{2}\sum_{k=1}^{2}(-1)^{i+j+k}\ln\left[z_k+\left(x_i^2+y_j^2+z_k^2\right)^{1/2}\right] \\ B_y = -\dfrac{J_0}{4\pi}\sum_{i=1}^{2}\sum_{j=1}^{2}\sum_{k=1}^{2}(-1)^{i+j+k}\left\{\arctan\left[\dfrac{x_i y_j}{z_k\left(x_i^2+y_j^2+z_k^2\right)^{1/2}}\right]+\arctan\left[\dfrac{y_j z_k}{x_i\left(x_i^2+y_j^2+z_k^2\right)^{1/2}}\right]\right\} \\ B_z = -\dfrac{J_0}{4\pi}\sum_{i=1}^{2}\sum_{j=1}^{2}\sum_{k=1}^{2}(-1)^{i+j+k}\ln\left[x_i+\left(x_i^2+y_j^2+z_k^2\right)^{1/2}\right] \end{cases}$$

(Equation 5)

Where J_0 is the mode of the residual magnetic vector of the material; i, j, and k are the coordinate vectors in the x, y, and z directions, respectively; $x_1 = x$; $x_2 = x\text{-}a$; $y_1 = y$; $y_2 = y\text{-}b$; $z_1 = z$; $z_2 = z\text{-}h$; a, b, and h are the side lengths of the rectangular permanent magnet in the x-, y-, and z axis directions, respectively.

According to the above analysis, the static magnetic field of any permanent magnet in space is only related to its size and magnetization direction, and the interaction of external magnetic fields of multiple permanent magnets conforms to the linear superposition law.[27] Therefore, after establishing the analytical formula of the magnetic field of a single rotating permanent magnet, and according to the feasibility of the magnetic field vector decomposition, the magnetic field of each array element is decomposed and superposed, and the radiation field model of the antenna array can be established.

Under the coordinate system of the linear array shown in Figure 2, the local coordinate system of the ith rotating permanent magnet array element is equivalent to the global coordinate system obtained by one translation and one rotation. Let $P(x_0,y_0,z_0)$ be a point under the global coordinate system $O\text{-}xyz$, which corresponds to point $P^{(i)}(x_0^{(i)},y_0^{(i)},z_0^{(i)})$ under the local coordinate system $O^{(i)}\text{-}x^{(i)}y^{(i)}z^{(i)}$ (i = 1,2, ⋯,n) of each array element. According to the simplified calculation formula of the Boschal model of three-dimensional coordinate transformation, it can be obtained that the transformation equation of point $P(x_0,y_0,z_0)$ inverse transformation into point $P^{(i)}(x_0^{(i)},y_0^{(i)},z_0^{(i)})$ is:

$$\begin{bmatrix} x_0^{(i)} \\ y_0^{(i)} \\ z_0^{(i)} \end{bmatrix} = \begin{bmatrix} x_0 \\ y_0 \\ z_0 \end{bmatrix} + \begin{bmatrix} 1 & 0 & 0 & 0 & -z_0 & y_0 & x_0 \\ 0 & 1 & 0 & z_0 & 0 & -x_0 & y_0 \\ 0 & 0 & 1 & -y_0 & x_0 & 0 & z_0 \end{bmatrix} \cdot \begin{bmatrix} -(i-1)d\cdot\cos\beta^{(i)} \\ (i-1)d\cdot\sin\beta^{(i)} \\ 0 \\ 0 \\ 0 \\ -\beta^{(i)} \\ 0 \end{bmatrix} \quad \text{(Equation 6)}$$

This leads to the fact that the coordinate form of $P^{(i)}$ is:

$$P^{(i)}\left(x_0{}^{(i)}, y_0{}^{(i)}, z_0{}^{(i)}\right) = \begin{bmatrix} x_0 - y_0\beta^{(i)} - d\cos\left(\beta^{(i)}\right)(i-1) \\ y_0 + x_0\beta^{(i)} + d\sin\left(\beta^{(i)}\right)(i-1) \\ z_0 \end{bmatrix} \quad \text{(Equation 7)}$$

By introducing the transformed coordinate $P^{(i)}$ into the element radiation theoretical formula, the magnetic field of the array element at $P(x_0,y_0,z_0)$ in the global coordinate system can be obtained. By analogy, the time-varying magnetic field intensity of each array element can be obtained. The magnetic field intensity is combined by three components after vector superposition, that is, the total time-varying magnetic field intensity of the rotating permanent magnet array with n elements under the global coordinate system $P(x_0,y_0,z_0)$ is:

$$\overrightarrow{B(P)} = \frac{B_0 V}{4\pi R^{(i)3}}\left[\sum_{i=1}^{n} 2\sin\theta\cos\left(\varphi^{(i)}+\gamma(t)^{(i)}\right)\overrightarrow{a_R} - \sum_{i=1}^{n}\cos\theta\cos\left(\varphi^{(i)}+\gamma(t)^{(i)}\right)\overrightarrow{a_\theta} - \sum_{i=1}^{n}\sin\left(\varphi^{(i)}+\gamma(t)^{(i)}\right)\overrightarrow{a_\varphi}\right]$$

(Equation 8)

Optimization of key parameters of coaxial linear array

Based on the above analytical model, the radiation field of the planar array is mainly influenced by the number of elements *n*, the element spacing *d* and the physical parameters of the permanent magnet material itself. Because the permanent magnet material imposes higher requirements on material science, we will use the control variable method to investigate the first two separately.

Optimization of array element spacing. According to Equation 8, arrays of one array element, two array elements, three array elements and four array elements are used for the study. The initial phase difference of the array elements is 0. The size of the permanent magnet array element in the two-array element is 60 × 30 × 30 mm. Keep the total volume of the permanent magnets in the other array groups the same as the two-array element array. The magnetization direction of the permanent magnets is all chosen in the length direction, the rotation frequency is chosen to be 75Hz, and the array element spacing is chosen to be 90–1200 mm (3/2*a*∼20*a*, *a* is the length dimension of the permanent magnet array element). The relationship between the array element spacing and the time-varying magnetic field strength at 50m is plotted as shown in Figure 3. The ordinate represents the first derivative of the total time-varying magnetic field intensity with respect to the array element spacing.

According to Figure 3, the time-varying magnetic field strength of the rotating permanent magnet array decays as a power-of-two function with the linear increase of the array element spacing. And the decay coefficient increases with the increase of the number of array elements. The maximum time-varying magnetic field strength is 86 *pT* when the spacing of the array elements is 90 mm (3/2*a*), which is approximately 99% of the time-varying magnetic field strength of a single rotating permanent magnet with the same total volume under the same conditions. The magnitude of the rate of change of the magnetic field strength is only 10^{-13} when observed at 50m using the permanent magnet array with the above parameters. Therefore, the effect of spacing can be disregarded when the ratio of spacing to communication distance is less than 0.02, but this parameter cannot be ignored when the ratio is larger (larger volume of individual permanent magnets, larger array element spacing, and closer communication distance).

Optimization of the number of array elements. Using permanent magnets with the same parameters as in the previous section, the array element spacing was selected to be 420 mm (i.e., 7*a*), 540 mm (i.e., 9*a*), and 660 mm (i.e., 11*a*). The number of array elements is 1–200, and the relationship between the number of array elements and the radiation gain (the radiation gain represents the gain value compared to the first group of "whole permanent magnet of the same volume") is plotted in Figure 4.

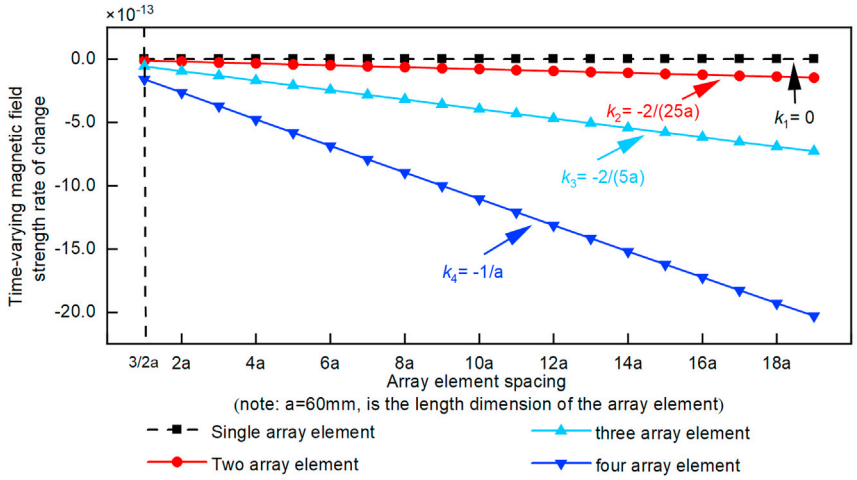

Figure 3. Relationship between the array spacing observed at 50 m for three sets of array element numbers

According to Figure 4, the number of permanent magnet array elements is roughly inversely proportional to the radiation gain. As the array element spacing increases, the radiation gain changes more rapidly. When the radiation gain reaches -3dB, the radiation field strength enhanced by the permanent magnet array is only half of the radiation strength of a single rotating permanent magnet of the same volume. In this case, an antenna array with a spacing of 7a can have up to 163 array elements, and an antenna array with a spacing of 11a can only have up to 104 array elements. Therefore, in the case of mechanical conditions allow, the smaller the array element spacing, the stronger the radiation capacity. If the number of array elements continues to increase, then the radiation efficiency will not reach 50% with respect to the same volume of individual permanent magnet. And it will increase the mechanical load, but the increased radiation intensity is very small. Therefore, we believe that the radiation gain reaches -3dB, which is the design limit of the number of array elements of the coaxial linear array.

Antenna array directivity. According to the radiation theory of permanent magnet mechanical antenna unit, the optimal radiation direction of its radiation field is distributed in the rotating plane, and the radiation field intensity decreases sharply in other directions perpendicular to the rotating plane.[28] In addition, when the receiving device uses a coil magnetic sensor, it is required to have good central symmetry for the incident wave. Therefore, to have better communication quality under the same radiation field, the radiation field directivity of antenna array is studied in this article.

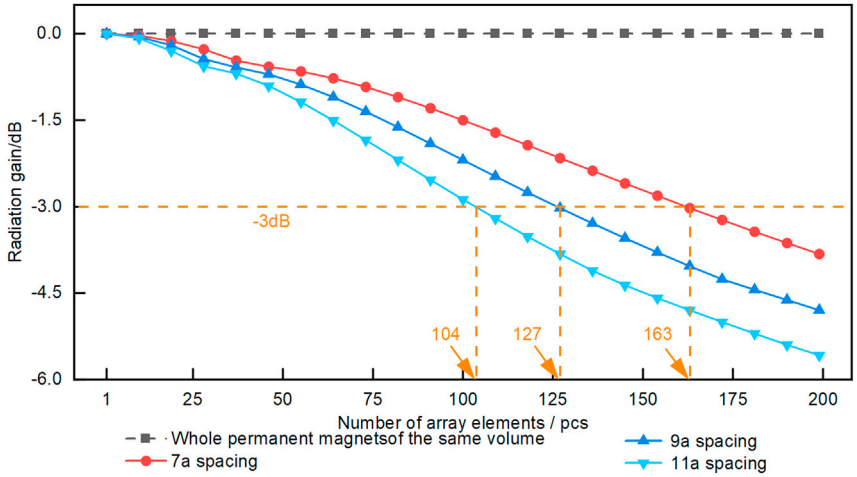

Figure 4. Relationship between the number of array elements observed at 50 m for the three sets of array spacing

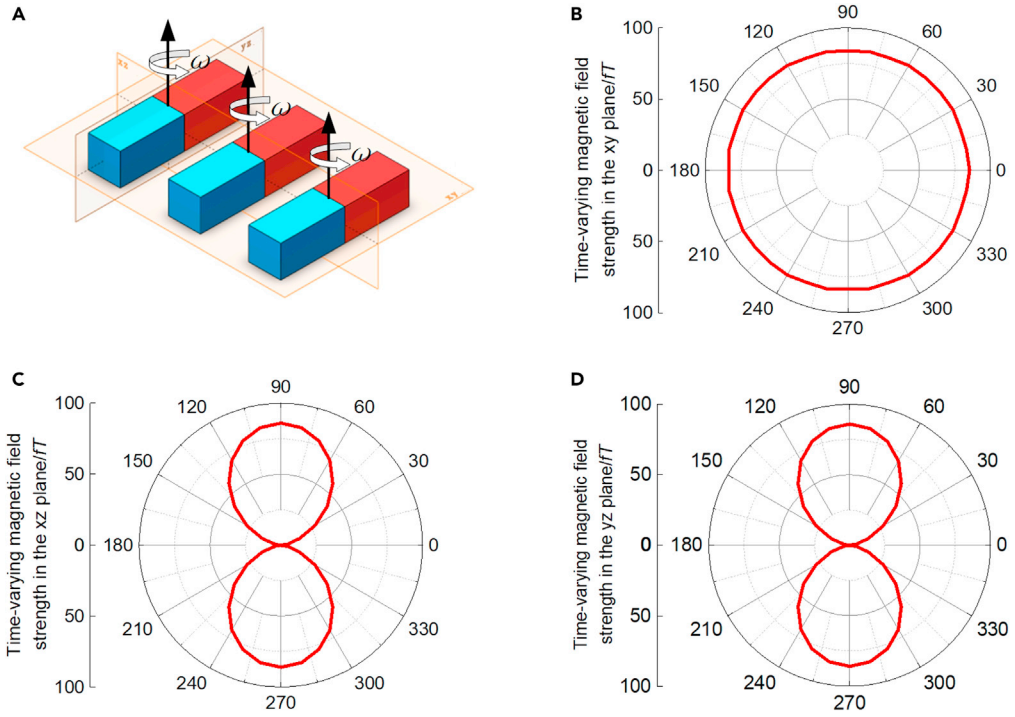

Figure 5. The relationship between the intensity of time-varying field and angle in the three orthogonal manifolds of the coaxial array element linear array

(A) Schematic diagram of the orthogonal three-part plane of the rotating permanent magnet array.

(B) The relationship between the intensity of the time-varying magnetic field in the xy-plane and the angle of φ.

(C) The relationship between the intensity of the time-varying magnetic field in the xz-plane and the angle θ.

(D) The relationship between the intensity of the time-varying magnetic field in the yz-plane and the angle θ.

Select the center of the transmitting antenna element as the origin of the pattern. The spacing of array elements is 90 mm. Select a circle with a radius of 500m as the standard circle. The antenna array pattern in polar coordinate system is shown in Figure 5.

According to the pattern, the intensity of the radiation field of the antenna array in the rotating plane is independent of the angle. In two planes perpendicular to the rotation plane, the position of the maximum radiation field appears at θ =90°. Therefore, for the super-low frequency transmitting antenna of coaxial linear array, the best receiving direction of the magnetic induction receiving sensor is the direction perpendicular to the rotating plane.

Array dynamics model

Unlike the electromagnetic wave radiated by the ESA antenna which is directly provided by the input modulated electrical signal, the electromagnetic wave radiated by the rotating permanent magnet mechanical antenna is mainly provided by the inherent remanence of the permanent magnet, and the auxiliary system only plays the role of signal modulation. Therefore, the stability of the antenna modulation system drive will directly determine the modulation quality of the communication signal.

The static magnetic field of the permanent magnet can form an input signal source similar to the excitation port of the electric antenna through mechanical rotation. Owing to the high remanence of permanent magnet, strong time-varying magnetic torque will be generated between adjacent elements behind the array, which is not conducive to the stable rotation of the array elements. And if the natural frequency of the antenna system is within the communication frequency range, it will cause resonance of the entire mechanical device, which is also unfavorable to the stable rotation of the element.

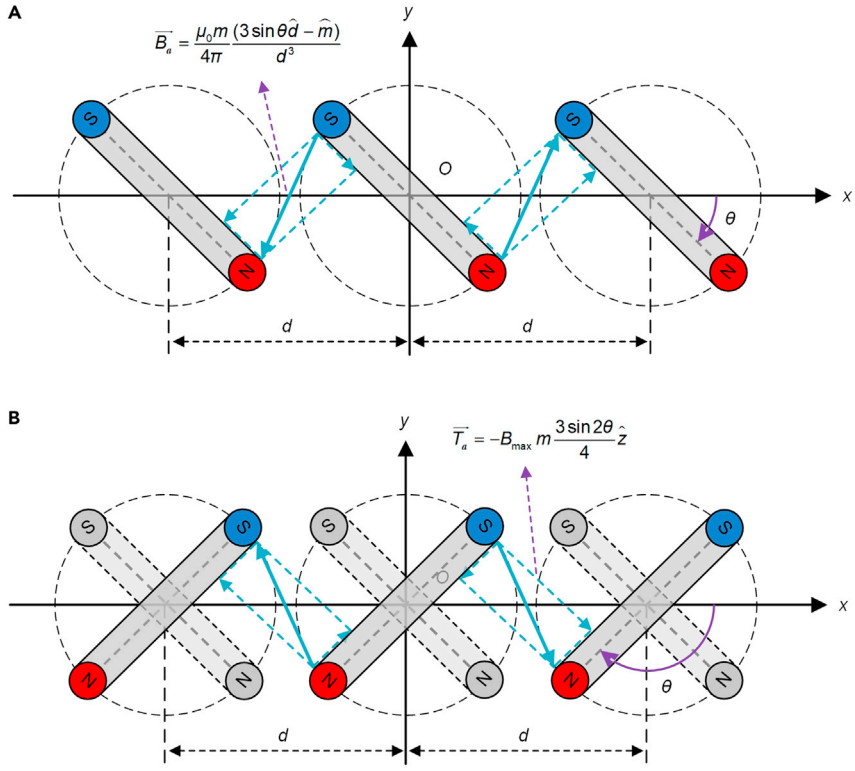

Figure 6. Physical model of permanent magnet array element and its equivalent motion model

(A) The array element is subjected to the inverse magnetic moment when the range $\theta \subset (0, \frac{\pi}{2})$.

(B) The array elements are subjected to positive magnetic moments when the range $\theta \subset (\frac{\pi}{2}, \pi)$.

In this chapter, differential equations of antenna system kinematics are established based on the theorem of moment of momentum, and then the resonance characteristics of the system are analyzed to optimize the input torque model of the system's smooth drive. Finally, through the optimization of model parameters, the stable driving of antenna system is realized, the signal quality of communication is improved and the frequency tolerance of communication signal is reduced.

Analysis of the magnetic moment of the array element

Taking the array of three elements as an example, the mechanical analysis of the antenna array is carried out in the common rotating plane. The N-pole of each element is horizontally to the right as the initial position, and the phase synchronization of the element is kept during rotation, and the rotation angle of each element relative to the x axis is θ. During the motion of the $\theta \subset (0, \pi)$ cycle, the magnetic moment between the elements is shown in Figure 6. In the second half of the $\theta \subset (\pi, 2\pi)$ cycle, the force of each array element is the same as in the first half cycle.

When the distance between the rotating centers of the array elements is d, the magnetic field force between two adjacent array elements can be expressed in the form of magnetic dipole field as:

$$\overrightarrow{B_a} = \frac{\mu_0 m}{4\pi}\frac{(3\sin\theta\hat{d} - \hat{m})}{d^3} \quad \text{(Equation 9)}$$

where μ_0 is vacuum permeability; m is the magnetic dipole moment; d is the spacing of adjacent elements.

The magnetic moment of adjacent array elements received by each array element is:

$$\overrightarrow{T_a} = -B_{max} m \frac{3\sin 2\theta}{4}\hat{z} \quad \text{(Equation 10)}$$

where B_{max} is the maximum magnetic field force subjected to during the movement of the array element, and its value can be determined by:

$$B_{max} = \frac{\mu_0 m}{2\pi d^3} \quad \text{(Equation 11)}$$

In the above array form, the middle element receives the force of the elements on both sides at the same time, and the magnitude and direction of the force are the same. From this, it can be deduced that the total magnetic moment of the middle array element is:

$$\overrightarrow{T_b} = 2\overrightarrow{T_a} = -B_{max} M_s V \frac{3\sin 2\theta}{2}\hat{z} \quad \text{(Equation 12)}$$

where M_s is the saturation magnetization strength.

System resonance frequency analysis

When the permanent magnet is polarized along the side length *a* direction, its rotational inertia J_a about the z_i axis passing through the center of mass is:

$$J_a = \frac{1}{12} m_a \left(a^2 + b^2\right) \quad \text{(Equation 13)}$$

where m_a is the permanent magnet mass; *a* is the polarization direction length of the permanent magnet; *b* is the cross-sectional edge length of the polarization direction of the permanent magnet.

During the rotating motion of the permanent magnet, Equation 14 can be deduced according to the theorem of moment of momentum:

$$J_a \ddot{\theta} = T_b + T_e \quad \text{(Equation 14)}$$

where T_b is the total magnetic moment experienced by the intermediate magnet; T_e is the external drive torque.

After rectification, the second order differential equation of the system can be obtained as:

$$\ddot{\theta} + \frac{9\mu_0 V {M_s}^2}{\pi \rho d^3 \left(a^2 + b^2\right)} \sin 2\theta = \frac{12 T_e}{\rho V \left(a^2 + b^2\right)} \quad \text{(Equation 15)}$$

Substituting the initial conditions: $\theta(0) = 0$, $\dot{\theta}(0) 2\pi f$, solving this second-order differential equation gives the equation of motion of the array element as:

$$\theta(t) = \frac{T_e}{3B_{max} M_s V} - \frac{e^{-\sigma_3}(T_e\sigma_4 + \sigma_2 + \sigma_1)}{6B_{max} M_s V \sigma_4} + \frac{e^{\sigma_3}(\sigma_2 - T_e\sigma_4 + \sigma_1)}{6B_{max} M_s V \sigma_4} \quad \text{(Equation 16)}$$

Among them,

$$\sigma_1 = \pi B_{max} M_s V f b^2 m_a \quad \text{(Equation 17)}$$

$$\sigma_2 = \pi B_{max} M_s V a^2 f m_a \quad \text{(Equation 18)}$$

$$\sigma_3 = \frac{6t\sigma_4}{m_a a^2 + m_a b^2} \quad \text{(Equation 19)}$$

$$\sigma_4 = \sqrt{-B_{max} M_s V m_a \left(a^2 + b^2\right)} \quad \text{(Equation 20)}$$

Then, the natural vibration frequency of the array element is:

$$f_n = \frac{\omega_n}{2\pi} = \frac{3M_s}{\pi d} \sqrt{\frac{\mu_0 V}{2\pi d \rho \left(a^2 + b^2\right)}} \quad \text{(Equation 21)}$$

where ρ is the density of the magnet; μ_0 is the vacuum permeability.

Substituting the parameters of the permanent magnet, we can obtain the intrinsic frequency of the system as $f_n = 19Hz$.

It can be seen from the above analysis that the natural frequency of the rotating permanent magnet is inversely proportional to the array element spacing d, and is related to the volume parameters a, b, h of the permanent magnet. When the natural frequency of the antenna system is within the communication frequency range, the system will form a resonance state. In this state, the interference of the magnetic torque between the array elements on the rotation speed is enhanced, and the stability of the array element rotation is sharply reduced. This state is unfavorable for stable communication. Therefore, the natural frequency of the system can be changed by adjusting the above parameters to make the communication frequency of the antenna system far away from the natural frequency f_n.

Analytical optimization model for drive torque

When the rotating permanent magnet antenna array uses 2FSK modulation mode for communication, theoretically, the modulation torque should be a square wave function. However, because of the large magnetic torque between the array elements, it is necessary to further optimize the modulation torque.

According to the analysis in the previous chapter, we can divide the driving moment T_e of the array element into two parts: One part is the resonant wave moment with the same frequency and complementary amplitude as the total magnetic moment received by the array element, and the other part is the velocity modulation moment. It can be expressed as:

$$T_e = \frac{3B_{max}M_sV}{2}\sin 2\theta + T_0 \quad \text{(Equation 22)}$$

where T_0 is the torque used for binary frequency shift keying modulation. By controlling the frequency and amplitude of T_0, the torque condition required by the drive system and the code rate required by communication can be achieved.

The second order differential equation of the antenna system is modeled, as shown in Figure 7. In the initial state of the system, increase a starting torque. The modulation torque T_0 of square wave function type is input during operation, and the simulation results are shown in Figure 8A. The motion of the system fluctuates greatly. The modulation torque T_0 and the resonant complementary torque are combined into T_e, which is used as the input of the total driving torque model. The simulation results are shown in Figure 8B.

The black line in Figure 8 reflects the torque of the rotating permanent magnet, including the external driving torque and the magnetic torque between the permanent magnet elements. The red line reflects the angular velocity change when the array element rotates. Because the second order differential equation of the system determines the acceleration and deceleration characteristics of the array element, the angular velocity of the array element will reach the specified communication angular velocity after a period of velocity change time, and finally realize the 2FSK modulation of the signal.

According to the simulation results, because of the addition of the resonant complementary torque, the force situation and the stability of the movement during the rotation of the array element have been greatly improved. The above analytical model of the system driving torque has feasibility and practical significance.

Experimental verification

Based on the above theoretical analysis, the overall communication system structure model of the super-low frequency mechanical antenna array is built as shown in Figure 9. The communication signal is modulated by 2FSK, and the signal generator is used to load the modulated signal on the carrier. Then the signal is sent to the frequency converter to drive the motor to realize the direct modulation of the signal. The magnetic field receiving sensor is designed as a three-axis orthogonal receiving coil based on electromagnetic induction effect. After the received signal is processed by the low noise signal processing module in the front end, the non-coherent demodulation of the super-low frequency communication signal is finally realized by cooperating with the digital processing circuit and the upper computer.

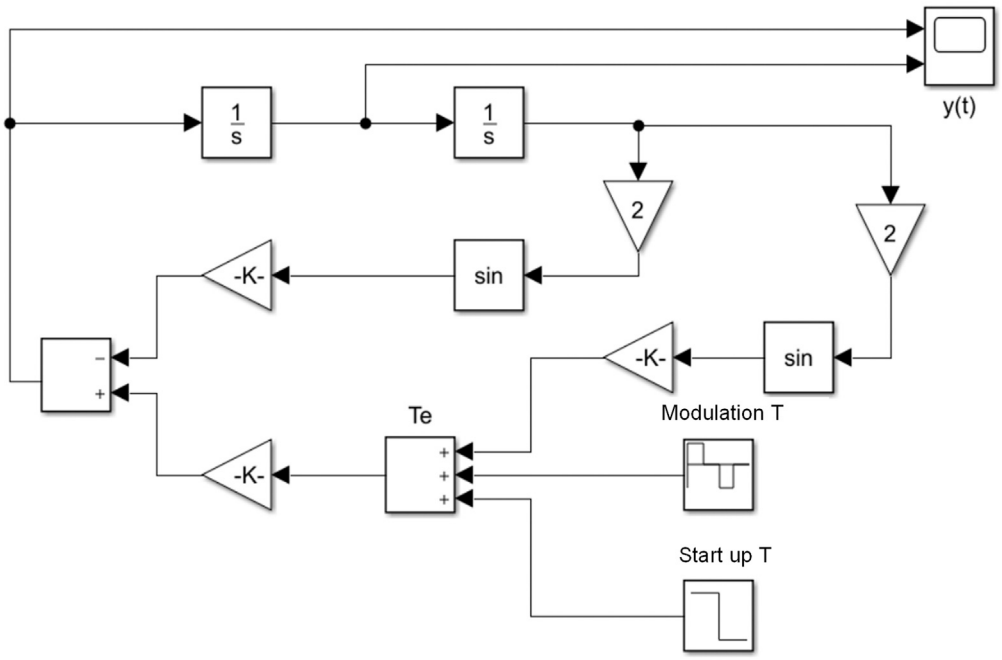

Figure 7. Simulink modeling simulation of the second order differential equations of motion

Three axis quadrature receiving coil can be equivalent to RLC circuit. Because the time-varying magnetic field generated by the rotating permanent magnet is a sinusoidal signal, the induced voltage generated by the terminal receiving coil can be determined by:[29]

$$V_a = N_a A_a \omega B \cos(\omega t) = 2\pi f N_a A_a B \cos\theta \quad \text{(Equation 23)}$$

where N_a is the number of turns of the coil, A_a is the area of the single-turn coil, ω is the angular velocity of the permanent magnet's rotation, f is the operating frequency, θ is the angle between the direction of incidence of the time-varying magnetic field and the axis of the coil.

Based on the above system structure model, the principal prototype of super-low frequency mechanical antenna is built as shown in Figure 10. The prototype is mainly composed of signal modulation drive module, rotating permanent magnet array antenna, signal receiving module and signal acquisition and processing module. The signal generator provides the driving signal for the high-voltage inverter, which constitutes the first part; The synchronous belt series drive rotating mechanism drives a plurality of permanent magnets to move, forming the second part; A three axis quadrature receiving coil with an impedance of 1Ω-1mH is designed as the signal receiving module; The fourth part is composed of the front low-noise signal amplifier and high-resolution oscilloscope, which collect the coil data and send it to the upper computer.

Calibration experiment of model parameters

Because the systematic error of the permanent magnet, coil, experimental environment and other experimental conditions will affect the accuracy of the experimental results, this section calibrates the undetermined parameters, environment and process correction coefficients in the antenna array radiation model by measuring the parameters of the permanent magnet at the transmitting end and the induced voltage of the receiving coil, and then determines the parameters of the permanent magnet material and the equivalent parameters of the coil as the benchmark for the next experiment.

Use the oscilloscope to collect the voltage signal received by the coil and obtain the frequency domain signal through FFT transformation. Thus, the presence of signals in each frequency band can be determined. Then, the signals in the communication frequency band are intercepted by band-pass filtering. The peak-to-peak value of filtered signal is determined by data statistics. According to the peak-to-peak

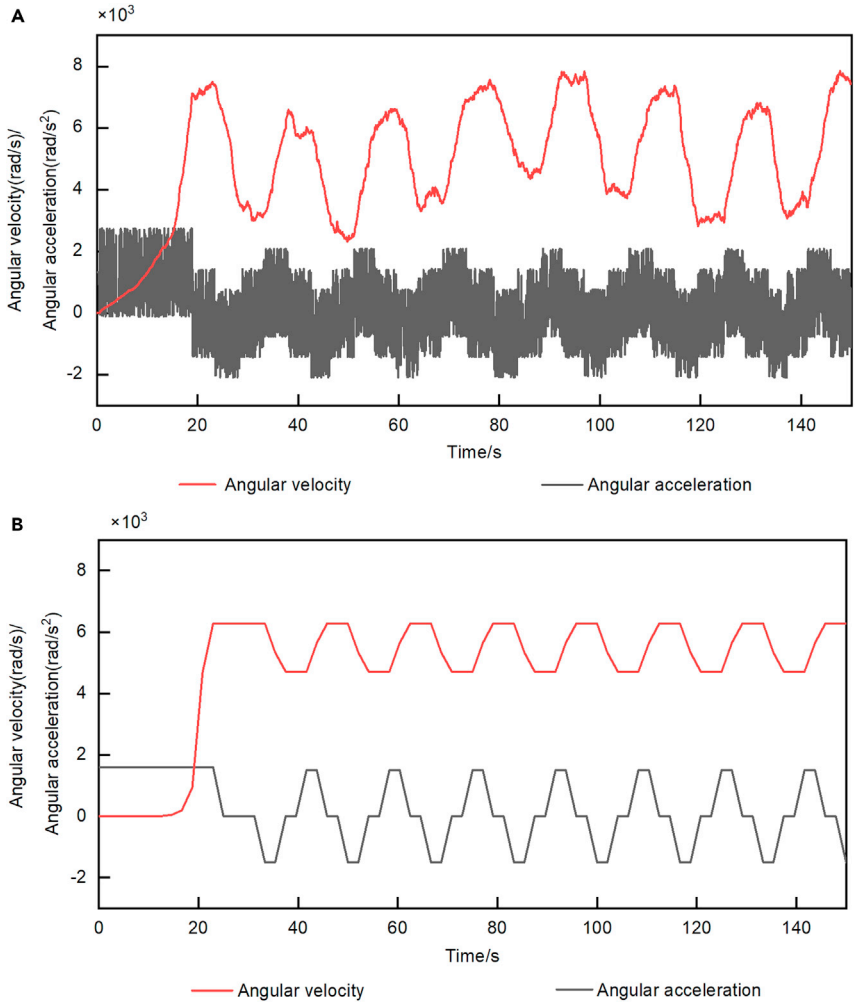

Figure 8. Comparison of simulation results of system drive torque model modulation

(A) Direct torque modulation simulation.

(B) Simulation of complementary torque modulation.

value of the signal, the equivalent time-varying magnetic field intensity detected by the coil can be obtained. Owing to the relative mechanical motion error of the prototype, such as slipping, there is a certain error in the actual measured communication frequency. The time-domain and frequency-domain signals measured in the experiment are shown in Figure 11 below.

A single rotating permanent magnet with magnetic brand N52 is used as the calibration object, and the rotation frequency is set to 75Hz. Use a coil with 21 turns and 0.6m side length to detect electromagnetic waves. The signals of time-varying magnetic field were detected at the places 2, 4 and 6 m away from the permanent magnet respectively, and they served as the control group. Specific experimental data are shown in Table 1.

On the one hand, there are errors in the physical parameters of permanent magnet materials, and on the other hand, the coils wound by hand are not arranged neatly, which will cause errors in the original parameters. According to the permanent magnet radiation model and coil detection model, each equivalent parameter can be recalibrated to calibrate the parameters of the analytical model. The equivalent coefficients under experimental conditions are shown in Table 2.

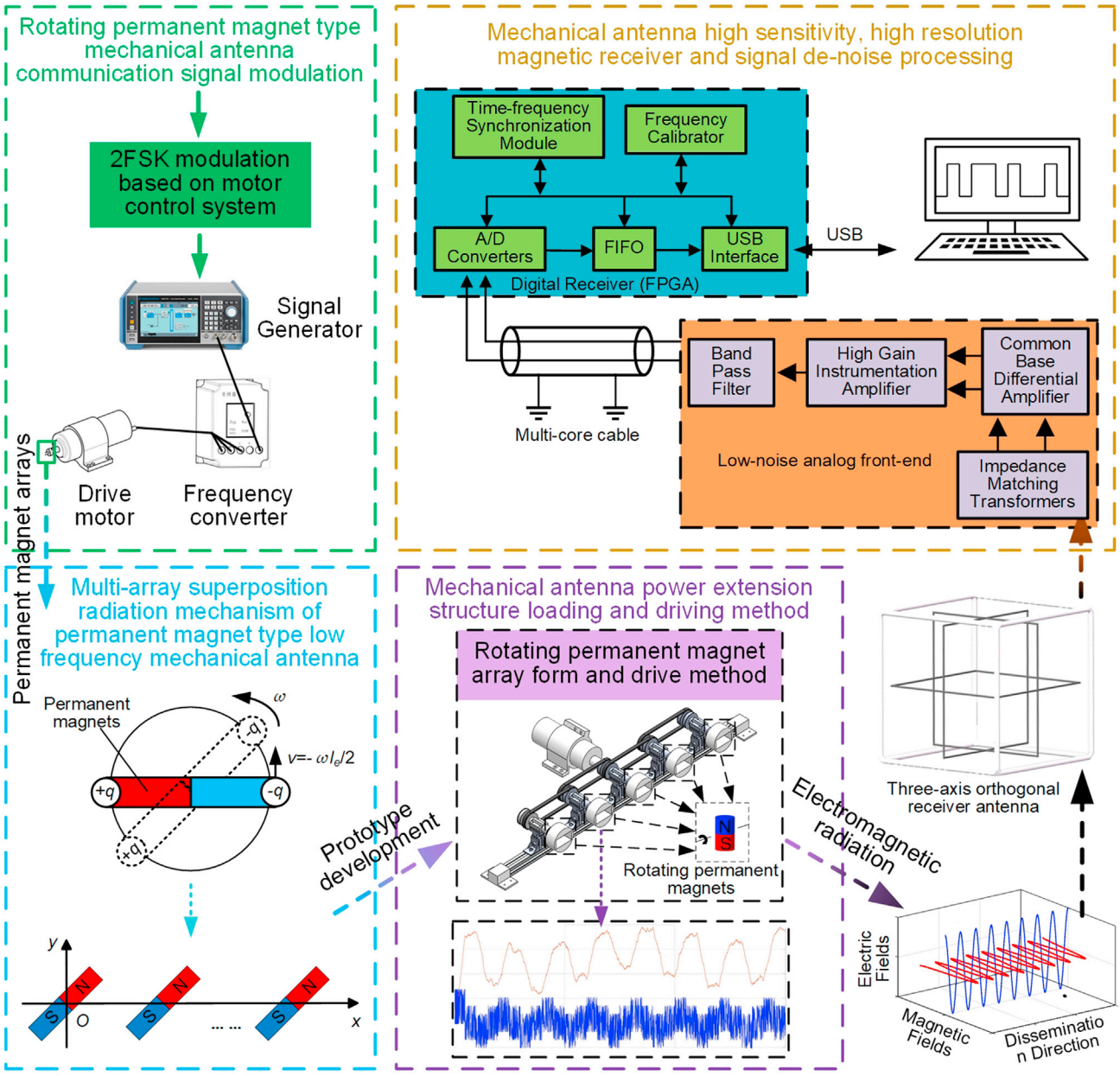

Figure 9. SLF mechanical antenna array communication system composition

Experiment on the influence of array element spacing

To verify the influence of array element spacing on the time-varying magnetic field intensity of coaxial linear array radiation, the experimental scheme is designed as follows. The receiving coil is placed on the vertical plane of the rotating plane of the permanent magnet array element. Keep the initial phase difference of the elements as 0, and change the spacing of the elements in turn. Using the oscilloscope and the pre-low-frequency amplifier, obtain the induced potential U of the three-axis orthogonal receiving coil. Five groups of time-varying magnetic field signals with different array element spacing d (d = 3/2a~9a, a is the length of permanent magnet array element) are analyzed, and their time-varying magnetic field intensity is calculated. The relationship between array element spacing and time-varying magnetic field intensity is shown in Figure 12.

Based on the experimental results, it can be concluded that the time-varying magnetic field strength decays by a third power as the detection distance increases. And with the increase of the spacing of the

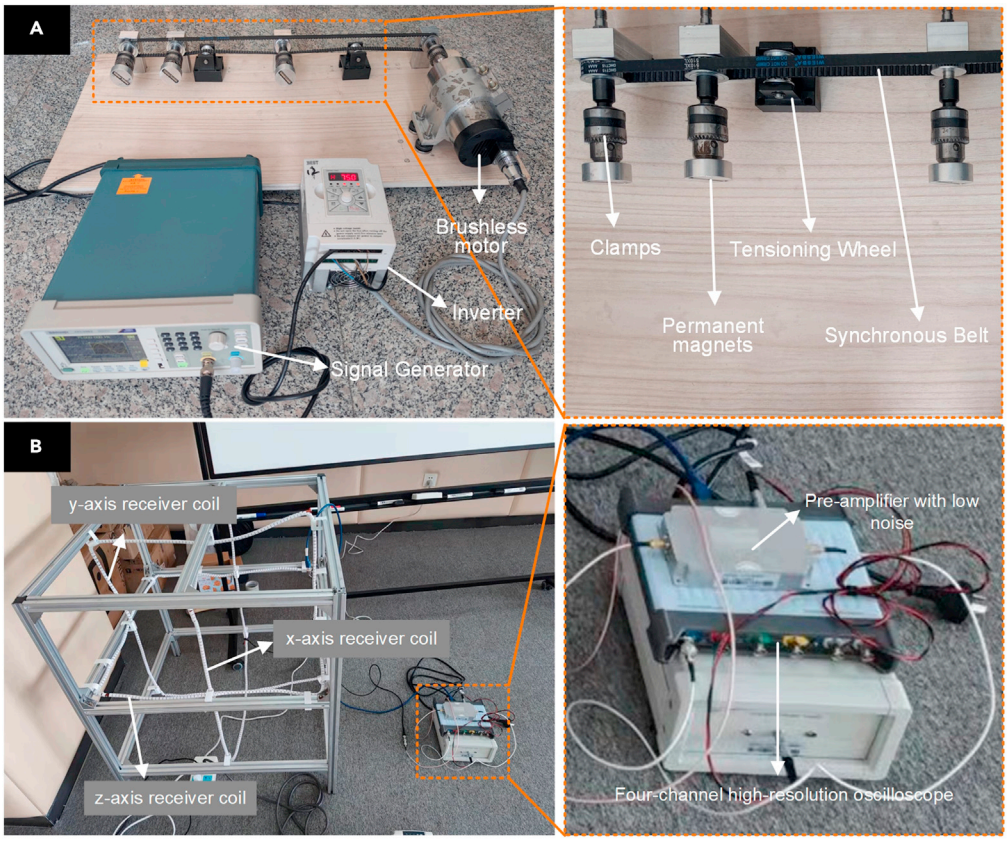

Figure 10. Rotating permanent magnet type super-low frequency mechanical antenna array prototype physical diagram

(A) Coaxial linear array transmitter.

(B) Three-axis orthogonal receiver.

array elements, the total time-varying magnetic field strength after the array decreases. However, with the increase of detection distance, the influence of element spacing on the total magnetic field strength decreases.

Now define the array attenuation rate as K, which represents the absolute value of the difference between the time-varying magnetic field strength under the two array parameters as a proportion of the original time-varying magnetic field strength, and the expression is:

$$K = \frac{|B_1 - B_2|}{B_1} \quad \text{(Equation 24)}$$

According to the experimental results, when the observation distance is 0.5m, and the spacing difference between the two groups of elements is 7.5 times the length size of the permanent magnet (that is, the element spacing changes from $3/2a$ to $9a$), the array attenuation rate $K \approx 62\%$. When the observation range increases to 4m, $K \approx 1.5\%$. Therefore, when the communication distance is close, the component spacing has a greater influence on the strength of the total radiated magnetic field. However, when the communication distance reaches 1 km, the array decay rate K will theoretically converge to zero.

Experiment on the influence of the number of array elements

To verify the influence of the number of elements on the time-varying magnetic field intensity radiated by the coaxial linear array, the experimental scheme is designed as follows. The receiving coil is placed on the vertical plane of the rotating plane of the permanent magnet array element. Keep the initial phase difference of array elements as 0, the spacing of array elements as 90 mm, and the observation distance as 4m. Increase the number of array elements n in turn to form experimental control group 1. Keep other

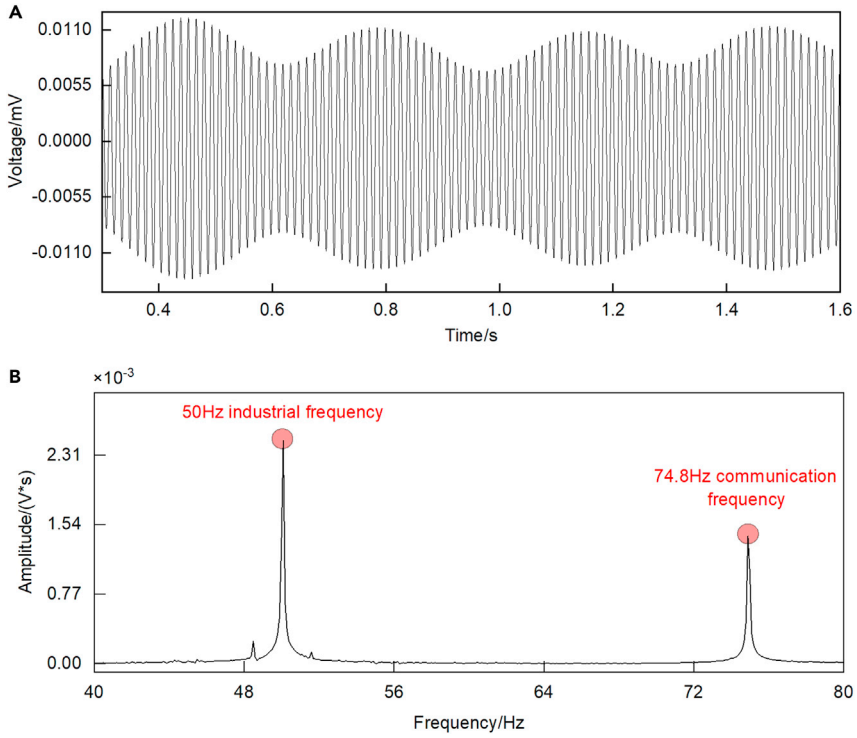

Figure 11. Rotating permanent magnet radiation time domain signal and FFT frequency domain signal

(A) Receiving coil time domain voltage.

(B) Frequency domain amplitude after FFT transformation.

experimental conditions unchanged, increase the number of array elements *n* in turn, adjust the observation distance of each group, so that the time-varying magnetic field intensity of observation points is 1.418×10^{-9} T, forming experimental control group 2. Compare the data obtained from experiment group 1 and experiment group 2 with a single rotating permanent magnet with a volume of *n* times to obtain the relationship between them, as shown in Figure 13.

According to the experimental data analysis, when the number of elements is small, the superimposed time-varying magnetic field strength of the permanent magnet array increases linearly with the number of elements. The third power of the observed distance increases linearly with the number of elements. The array attenuation rate $K \approx 23.56\%$ because of the permanent magnets is broken into multiple individuals. When the sensitivity of the detection reaches 50 *fT*@75Hz, the volume of a single rotating permanent magnet required for 1 km communication is about 500 cm^3. When this level of communication is performed using the array scheme of this experiment, the total volume of permanent magnets required is approximately 654 cm^3.

Drive torque model experiment

The existing ESA antenna generally controls the output voltage and current frequency through a modulator. However, the mechanical antenna can directly change the movement state of the radiation source

Table 1. Experimental data on radiation from individual permanent magnets

Permanent magnet size/mm	Detection distance/m	Detecting coil voltage amplitude/V	Experimental time-varying magnetic field strength/T
30 × 30 × 60	2	1.32×10^{-4}	5.93×10^{-8}
	4	1.641×10^{-5}	7.36×10^{-9}
	6	4.913×10^{-6}	2.19×10^{-9}

Table 2. Equivalent calibration parameters of the permanent magnet radiation model

Calibration parameters	Calibration coefficient value
Equivalent coefficient of remanent magnetization of permanent magnet materials	0.73
Receiving coil size equivalence factor	0.83
Receiving coil turns equivalence factor	0.59

to achieve signal modulation and information loading. For this working property, the direct modulation method with constant envelope, such as FSK and MSK, is mainly used at present. The accuracy and stability of the mechanical movement of the permanent magnet array will directly affect the quality of the digital signal. Therefore, high requirements are put forward for the stable driving of the antenna system.

To verify the drive torque model optimized in this article and the influence on the stability of the mechanical system drive of the antenna array, the constant torque square wave function drive model and the harmonic complementary modulation torque drive model are used in turn to provide 75Hz frequency drive torque for the antenna array system, forming an experimental control group. The implementation of the harmonic complementary modulation drive can be divided into three steps. First, a pre-designed harmonic complementary modulation torque function model (one cycle) based on the operating frequency is generated using MATLAB software; Second, the generated waveform data is imported into the signal generator, and the signal period and peak range are set to generate a drive signal with a peak within ±10V; Third, the inverter is set to the external signal drive mode and the signal from the signal generator is fed to the inverter to control the rotational motion of the motor according to the pre-designed drive model. Use an oscilloscope to collect the data received by the induction coil, observe the time-frequency domain diagram of the signal through STFT transformation, and compare the stability of the signal. The experimental results are shown in Figure 14.

From the analysis of the experimental data, when the drive model is driven by a constant-torque square-wave function, the frequency of the signal jitters around 75Hz, and the frequency-domain tolerance of the signal is about 17Hz. When the optimized torque model is introduced, the jitter of the signal frequency around 75Hz is reduced significantly. The frequency-domain tolerance of the signal is only 9Hz, which

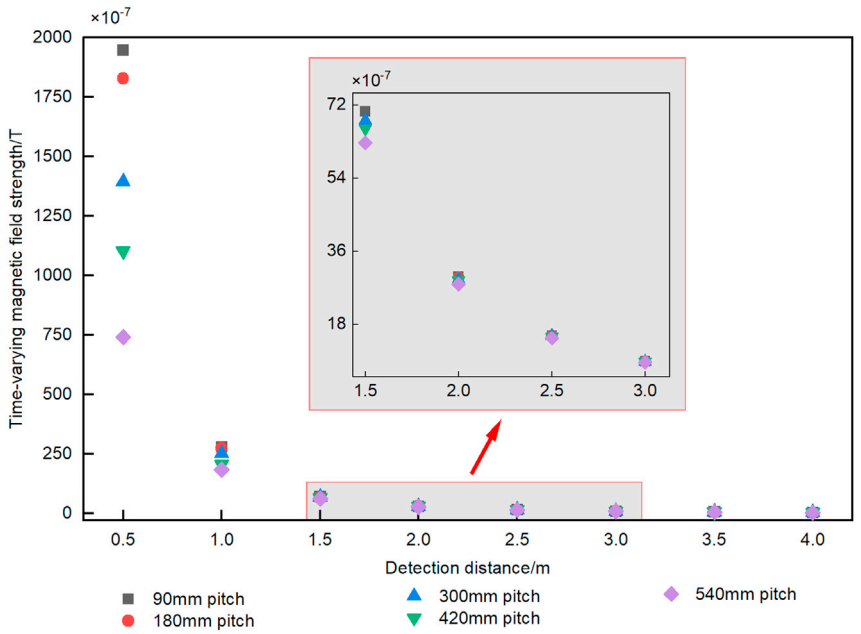

Figure 12. Relationship between array element spacing and array time-varying magnetic field strength

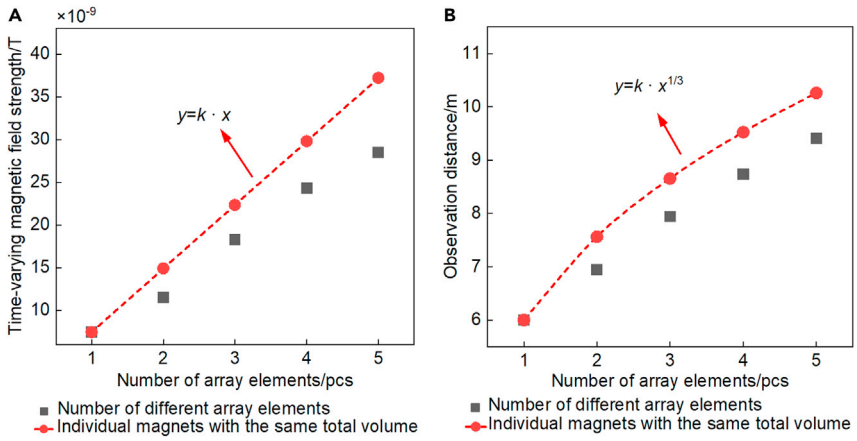

Figure 13. Relationship between the number of array elements and the array time-varying magnetic field strength and observable distance

(A) Radiation intensity of the array at the same observation distance.

(B) Observation distance for the same radiation intensity of the array.

improves 47%. The optimized driving model improves the signal stability, reduces the load of the motor when the whole device is working, and improves the communication efficiency of the antenna. From the aspect of signal stability, the validity and feasibility of the modulation drive torque built in this article are verified.

2FSK digital frequency communication experiment

To verify the information loading capability of the antenna array and the feasibility of digital communication, a coaxial linear array of four array elements is used as the radiation source and the time-varying magnetic field signal is detected at 76m using a three-axis orthogonal receiver coil. Constant envelope modulation is achieved by real-time control of the permanent magnet speed, in other words, the frequency modulation corresponds to the control of the average speed *n* to achieve.

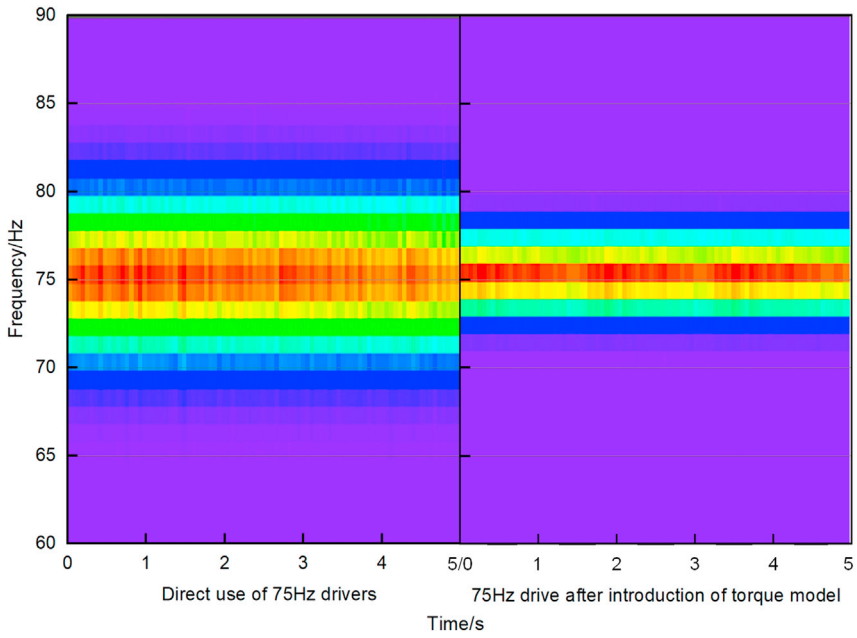

Figure 14. Time and frequency domain diagram of the measured signal of the modulated torque drive model

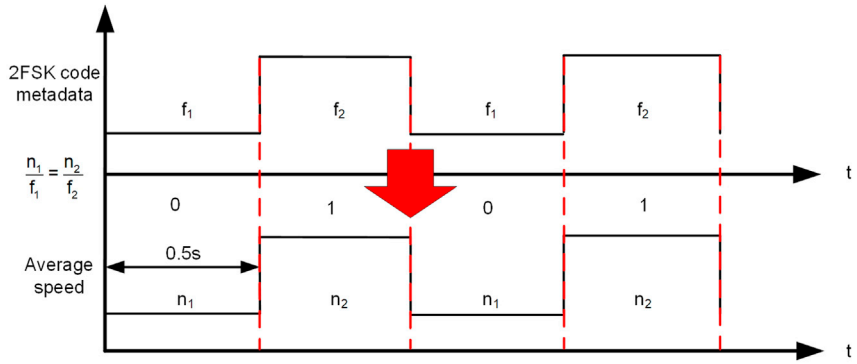

Figure 15. Schematic diagram of speed control signal generation with 2FSK

Based on the control mode for the average speed *n*, Figure 15 shows a schematic diagram of the speed control signal generated from the 2FSK code metadata. In the 2FSK modulation mode, the control waveform of the rotational speed is a square wave function. The first rpm n_1 and the second rpm n_2 are 4500rpm (f_1 = 75Hz) and 7500rpm (f_2 = 125Hz), respectively. The duration of each RPM is 0.5s and cycles alternate.

Figure 16 is the time-frequency domain diagram of the time-varying magnetic field signal obtained in the experiment, which mainly includes 75Hz, 125Hz and 50Hz power frequencies and their higher harmonic components. My guess as to the reason for the apparent variation in the received voltage amplitude during the measured time is as follows. According to the law of electromagnetic induction, the magnitude of the induced voltage generated by the coil is proportional to the operating frequency. In addition, the magnitude of the time-varying magnetic field generated by the permanent magnet type mechanical antenna is independent of the operating frequency. Therefore, when detecting the same strength of magnetic field at the same point, the amplitude of the induced voltage will be different for different operating frequencies. Second, because the coil sensor can be equated to an RLC circuit, it will generate electromagnetic oscillations during operation, which turns the outer envelope of the two operating frequency signals into a sinusoidal form.

From the STFT results, it can be seen that the trend of the waveform of the signal is consistent with that of the speed control signal. Because the speed of the drive motor is transient, there is a change process when the frequency changes Δt. In the time-frequency domain diagram, the frequency changes are shown as diagonal lines. According to the experimental results, the rise time of frequency is 0.12s, the fall time of frequency is 0.14s, and the total change time is Δt = 0.26s。 Therefore, in the 2FSK communication system of this experiment, the bit error rate of the signal is 6.19%, and the communication code rate is 1bps. The experimental results show the same trend with the preset conditions, and verify the effectiveness and feasibility of the super-low frequency mechanical antenna communication scheme based on the rotating permanent magnet array described in this article from the practical application level.

Results and discussion

Aiming at the problems of large size, large power consumption, low efficiency, and complex structure of traditional low-frequency antennas, this article proposes a large-scale array super-low frequency antenna based on rotating permanent magnets. The array parameters and motion equations of the permanent magnets are introduced to establish the relationship between the antenna array parameters and the radiation's time-varying magnetic field strength. By analyzing the dynamics of the antenna array, the mechanical drive model of the system is established, and finally, the tolerance of the communication signal is reduced. Based on the directivity of the transmitting antenna, a prototype antenna array was made using permanent magnets with dimensions of 30 × 30 × 60 mm, and the time-varying magnetic field within a range of up to 76m was detected. A triaxial quadrature coil is used as a magnetic field sensor to receive electromagnetic wave signals. By fitting the detected signal with the theoretical model, the method proposed in this article to construct large-scale antenna arrays to achieve ultra-long-distance low-frequency communication is verified.

According to the theoretical and experimental results of this article, some characteristics of the coaxial array element linear arrays obtained from the decomposition of the basic grouping of planar arrays are derived.

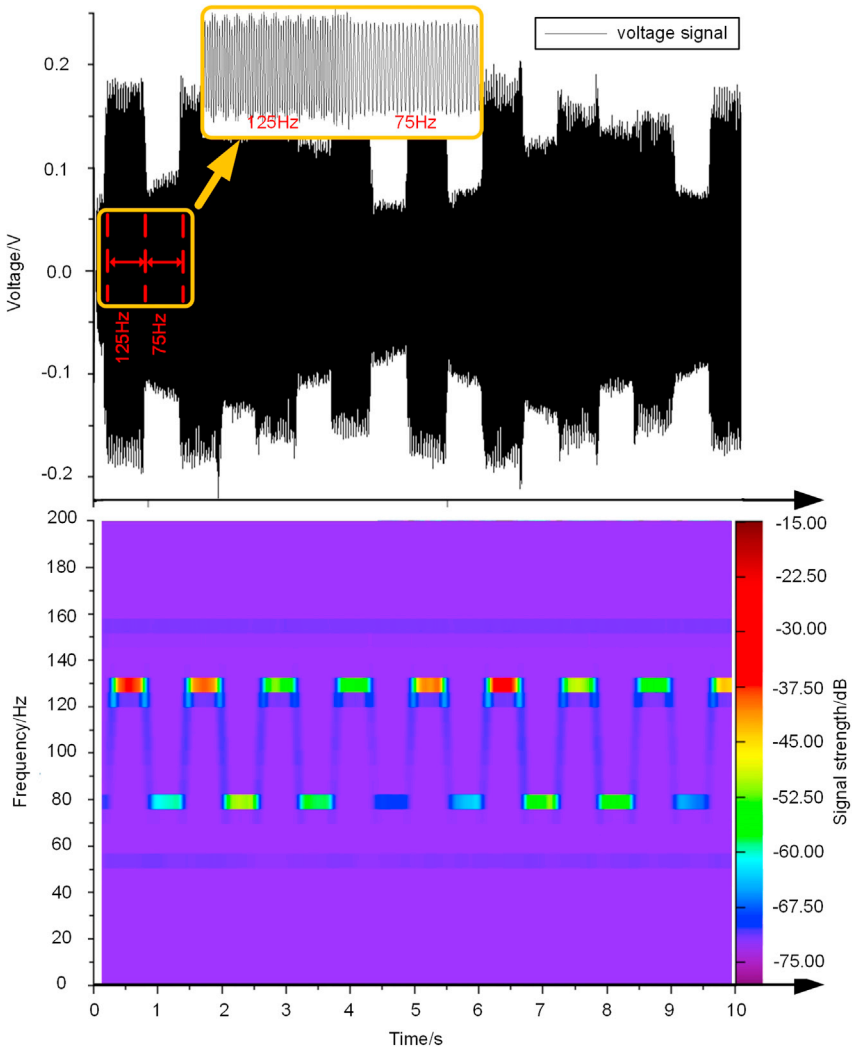

Figure 16. Time-frequency domain diagram of the measured signal corresponding to 2FSK

1) The antenna array propagates in its plane of rotation and has no directionality; Propagating in two planes perpendicular to its plane of rotation, the direction of the largest electromagnetic wave occurs at the intersection of the plane of rotation.

2) The spacing of the array elements is inversely proportional to the quadratic of the total intensity of the array's time-varying magnetic field, and the attenuation coefficient increases with the increase in the number of elements.

3) The number of permanent magnet array elements is roughly inversely proportional to the radiation gain (the radiation gain represents the gain value compared to the "whole permanent magnet of the same volume"). As the array element spacing increases, the radiation gain changes more rapidly, so the saturation point of the array is advanced. When the radiation gain reaches -3dB, the radiation field strength enhanced by the permanent magnet array is only 50% of the radiation strength of a single rotating permanent magnet of the same volume.

4) In near-distance super-low-frequency communication, the array element spacing has a greater impact on the overall radiation efficiency. However, when the communication distance reaches 1 km, there is almost no effect. When the observation distance is 4 m, the loss caused by the array spacing of 7.5 times the length of the permanent magnet can reach 1.5%. But this loss will tend to zero when the observation distance reaches 1 km.

5) When the total volume of permanent magnets is the same, the total number of split elements has a great influence on the total radiation efficiency of the array. When five elements are used to detect at 10m, the loss is about 23.56%.

6) By optimizing the drive torque model of the antenna mechanical system, the tolerance of the antenna communication signal is improved by 47%. Through the direct modulation of the antenna radiation source speed, constant envelope modulation such as FSK and MSK can be realized, and information loading can be completed to realize super-low-frequency communication.

STAR★METHODS

Detailed methods are provided in the online version of this paper and include the following:

- KEY RESOURCES TABLE
- RESOURCE AVAILABILITY
  - Lead contact
  - Materials availability
  - Data and code availability
- METHOD DETAILS

ACKNOWLEDGMENTS

This work was supported by the Equipment Advance Research Fund (No. 61405180302), National Natural Science Foundation of China (No. 51005029), National Key Development Project (No. 0120700), and Natural Science Foundation of Liaoning Province of China (No. 2023011055-JH3/107).

AUTHOR CONTRIBUTIONS

Conceptualization: X.W. and X.Y.; investigation: X.Y., X.W., and Z.L.; visualization: X.Y., X.W., and B.Z.; funding acquisition: X.W. and Z.C.; supervision: X.W. and Z.C.; writing–original draft: X.Y.; writing–review and editing: X.W., X.Y. and Z.C.

DECLARATION OF INTERESTS

The authors declare no competing interests.

Received: January 19, 2023
Revised: March 2, 2023
Accepted: April 20, 2023
Published: April 25, 2023

REFERENCES

1. Zhang, W. (2016). Development trend and analysis of submarine communication technology(in Chinese). Ship Electron. Eng. *1*, 13–16. https://doi.org/10.3969/j.issn.1672-9730.2016.06.004.

2. J. Lu, ed. (2013). ELF and SLF Radio Technology(in Chinese) (Harbin Engineering University Press).

3. Y. Yuan, ed. (2011). Propagation and noise of super-low frequency and extremely low frequency electromagnetic waves(in Chinese) (National Defense Industry Press).

4. Shi, W., Ye, X., and Hu, D. (2011). Super-low frequency radio communication technology and its application in submarine communication abroad(in Chinese). Digital Technol. Appl. 12–13.

5. Chu, L.J. (1948). Physical limitations of omni-directional antennas. J. Appl. Phys. *19*, 1163–1175. https://doi.org/10.1063/1.1715038.

6. De Medeiros, L.H., Reyne, G., Meunier, G., and Yonnet, J.P. (1998). Distribution of electromagnetic force in permanent magnets. IEEE Trans. Magn. *34*, 3012–3015. https://doi.org/10.1109/20.717704.

7. Gong, S.R., Bao, L.L., and Liu, Y. (2018). A rotating-magnet based mechanical antenna (RMBMA) for ELF-ULF wireless communication. Animal Model. Exp. Med. *1*, 125–133. https://doi.org/10.2528/pierm18070204.

8. Shi, W., Zhou, Q., and Liu, B. (2019). Performance analysis of spinning magnet as mechanical antenna(in Chinese). Acta Phys. Sin. *68*, 314–324.

9. Zhou, Q., Yao, F., Shi, W., Hao, Z., Zheng, H., Liu, B., and He, P. (2020). Research on mechanism and key technology of mechanical antenna for low frequency transmission(in Chinese). Sci. Sin. Tech. *50*, 69–84.

10. Burch, H.C., Garraud, A., Mitchell, M.F., Moore, R.C., and Arnold, D.P. (2018). Experimental generation of ELF radio signals using a rotating magnet. IEEE Trans. Antennas Propag. *66*, 6265–6272. https://doi.org/10.1109/tap.2018.2869205.

11. Prasad, M.N.S., Selvin, S., Tok, R.U., Huang, Y., and Wang, Y. (2018). Directly Modulated Spinning Magnet Arrays for ULF Communications (IEEE), pp. 171–173. https://doi.org/10.1109/RWS.2018.8304977.

12. Selvin, S., Srinivas Prasad, M.N., Huang, Y., and Wang, E. (2017). Spinning Magnet Antenna for VLF Transmitting (IEEE), pp. 1477–1478. https://doi.org/10.1109/APUSNCURSINRSM.2017.8072781.

13. Bickford, J.A., Duwel, A.E., Weinberg, M.S., Mc N Abb, R.S., Freeman, D.K., and Ward, P.A. (2019). Performance of electrically small conventional and mechanical antennas. IEEE

Trans. Antennas Propag. *67*, 2209–2223. https://doi.org/10.1109/TAP.2019.2893329.

14. Brandsema, M.J., and Bufler, T.D. (2022). ELF-VLF transmissions via motion-induced radiation of charges. IEEE Trans. Antennas Propag. *70*, 9039–9050. https://doi.org/10.1109/tap.2022.3177503.

15. Cao, J., Tan, X.Y., Jia, N., Lan, D., Solco, S.F.D., Chen, K., Chien, S.W., Liu, H., Tan, C.K.I., Zhu, Q., et al. (2022). Dual-band piezoelectric artificial structure for very low frequency mechanical antenna. Nanoscale *14*, 410–418. https://doi.org/10.1007/s42114-022-00431-4.

16. Xu, J., Li, Z., Pan, X., Wen, X., Cao, J., Gong, W., Yang, S., Lei, M., Yao, F., and Bi, K. (2023). Ultra-wideband electrostrictive mechanical antenna. Adv. Funct. Mater. *33*, 2210868. https://doi.org/10.1002/adfm.202210868.

17. Dong, C., He, Y., Li, M., Tu, C., Chu, Z., Liang, X., Chen, H., Wei, Y., Zaeimbashi, M., Wang, X., et al. (2020). A portable very low frequency (VLF) communication system based on acoustically actuated magnetoelectric antennas. IEEE Antennas Wirel. Propag. Lett. *19*, 398–402. https://doi.org/10.1109/lawp.2020.2968604.

18. Nan, T., Lin, H., Gao, Y., Matyushov, A., Yu, G., Chen, H., Sun, N., Wei, S., Wang, Z., Li, M., et al. (2017). Acoustically actuated ultra-compact NEMS magnetoelectric antennas. Nat. Commun. *8*, 296. https://doi.org/10.1038/s41467-017-00343-8.

19. Cui, Y., Wang, C., Song, X., Wu, M., Zhang, Q., Yuan, H., and Yuan, Z. (2023). A survey of mechanical antennas applied for low-frequency transmitting. iScience *26*, 105832. https://doi.org/10.1016/j.isci.2022.105832.

20. Sugimoto, S. (2011). Current status and recent topics of rare-earth permanent magnets. J. Phys. D Appl. Phys. *44*, 064001. https://doi.org/10.1088/0022-3727/44/6/064001.

21. Jiang, Q., and Zhong, Z. (2017). Research and development of Ce-containing Nd2Fe14B-type alloys and permanent magnetic materials. J. Mater. Sci. Technol. *33*, 1087–1096. https://doi.org/10.1016/j.jmst.2017.06.019.

22. Thanalakshme, R.P., Kanj, A., Kim, J., Wilken-Resman, E., Jing, J., Grinberg, I.H., Bernhard, J.T., Tawfick, S., and Bahl, G. (2022). Magneto-mechanical transmitters for ultralow frequency near-field data transfer. IEEE Trans. Antennas Propag. *70*, 3710–3722. https://doi.org/10.1109/tap.2021.3137244.

23. Cui, J., Ormerod, J., Parker, D., Ott, R., Palasyuk, A., McCall, S., Paranthaman, M.P., Kesler, M.S., McGuire, M.A., Nlebedim, I.C., et al. (2022). Manufacturing processes for permanent magnets: Part I—sintering and casting. JOM *74*, 1279–1295. https://doi.org/10.1007/s11837-022-05156-9.

24. Wang, X., Zhang, W., Zhou, X., Cao, Z., and Quan, X. (2020). Radiation characteristics of rotating magnetic dipole super-low frequency transmitting antenna(in Chinese). Acta Armamentarii *41*, 2055–2062. https://doi.org/10.3969/j.issn.1000-1093.2020.10.015.

25. Lee, M.G., Lee, S.Q., and Gweon, D.-G. (2004). Analysis of Halbach magnet array and its application to linear motor. Mechatronics *14*, 115–128. https://doi.org/10.1016/s0957-4158(03)00015-1.

26. P. Xia, ed. (2000). Permanent magnet mechanism(in Chinese) (Beijing University of Technology Press).

27. Li, X., Xu, J., and Liu, H. (2008). Three-dimensional magnetic field distribution around a rectangular permanent magnet(in Chinese). J. Beijing Univ. Technol. *034*, 1–6.

28. Nagaraja, S.P.M. (2017). Going beyond Chu's Limit: ULF Radiation with Directly Modulated Spinning Magnet Arrays (University of California). https://escholarship.org/uc/item/0755g3wm.

29. Wang, X.Y., Wang, Y., Wu, Q., Liu, J.J., Liu, Y., Pan, D.H., Qi, W., Wang, L.Z., Yan, J.J., Xu, Y.P., et al. (2021). Research on super-low frequency mechanical antenna model and experimental study of magnetic sensor coil(in Chinese). Acta Pharmacol. Sin. *42*, 824–831. https://doi.org/10.12263/DZXB.20200254.

STAR★METHODS

KEY RESOURCES TABLE

REAGENT or RESOURCE	SOURCE	IDENTIFIER
Software and algorithms		
MATLAB, version 2018b	MathWorks, Inc.	RRID:SCR_001622
Origin, version 9.8.0.200	OriginLab Corporation	RRID:SCR_014212
SOLIDWORKS, version 2020	Dassault Systemes	RRID: AB_2313773

RESOURCE AVAILABILITY

Lead contact

Further information and requests for resources and reagents should be directed to and will be fulfilled by the lead contact, Xiaoyu Wang (xiaoyuw@djtu.edu.cn).

Materials availability

This study did not generate new unique reagents.

Data and code availability

- All data reported in this paper will be shared by the lead contact upon request.
- This paper does not report original code.
- Any additional information required to reanalyze the data reported in this paper is available from the lead contact upon request.

METHOD DETAILS

The magnetic grade of the permanent magnet material is N52. The dimensions of the individual permanent magnets used in the experiments were 30×30×60mm. The permanent magnet jig is made of aluminum alloy and machined to shape. The detection coil uses a 1mm diameter copper wire. The side length of the coil is 600mm and the number of turns is 21 turns. The crucial array parameters analysis in optimization of key parameters of coaxial linear array and the driving torque simulation in analytical optimization model for drive torque were computed using MATLAB software. The experimental data filtering, FFT transformation, and STFT transformation of experimental verification were computed using Origin software. The prototype's structural design for experimental verification was created using SOLIDWORKS software.